

ORIGINAL RESEARCH

Activation of the ATF6 (Activating Transcription Factor 6) Signaling Pathway in Neurons Improves Outcome After Cardiac Arrest in Mice

Yuntian Shen , PhD*; Ran Li, MD*; Shu Yu, PhD; Qiang Zhao , MD; Zhuoran Wang, PhD; Huaxin Sheng, MD; Wei Yang , PhD

BACKGROUND: Ischemia/reperfusion injury impairs proteostasis, and triggers adaptive cellular responses, such as the unfolded protein response (UPR), which functions to restore endoplasmic reticulum homeostasis. After cardiac arrest (CA) and resuscitation, the UPR is activated in various organs including the brain. However, the role of the UPR in CA has remained largely unknown. Here we aimed to investigate effects of activation of the ATF6 (activating transcription factor 6) UPR branch in CA.

METHODS AND RESULTS: Conditional and inducible sATF6-KI (short-form ATF6 knock-in) mice and a selective ATF6 pathway activator 147 were used. CA was induced in mice by KCl injection, followed by cardiopulmonary resuscitation. We first found that neurologic function was significantly improved, and neuronal damage was mitigated after the ATF6 pathway was activated in neurons of sATF6-KI mice subjected to CA/cardiopulmonary resuscitation. Further RNA sequencing analysis indicated that such beneficial effects were likely attributable to increased expression of pro-proteostatic genes regulated by ATF6. Especially, key components of the endoplasmic reticulum-associated degradation process, which clears potentially toxic unfolded/misfolded proteins in the endoplasmic reticulum, were upregulated in the sATF6-KI brain. Accordingly, the CA-induced increase in K48-linked polyubiquitin in the brain was higher in sATF6-KI mice relative to control mice. Finally, CA outcome, including the survival rate, was significantly improved in mice treated with compound 147.

CONCLUSIONS: This is the first experimental study to determine the role of the ATF6 UPR branch in CA outcome. Our data indicate that the ATF6 UPR branch is a prosurvival pathway and may be considered as a therapeutic target for CA.

Key Words: brain ischemia ■ ER stress ■ ER-associated degradation ■ neuroprotection ■ RNA-Seq ■ transgenic mice

Protein homeostasis (or proteostasis) is impaired under many pathologic conditions of major clinical significance, and a large number of studies have focused on impaired proteostasis in such chronic diseases as diabetes mellitus, cancer, and neurodegenerative diseases.^{1,2} Notably, mounting evidence indicates that disrupted proteostasis also plays a critical role in the pathogenesis of acute diseases, especially ischemia/reperfusion injury in various organs.^{3,4} It has

been proposed that a promising therapeutic strategy to protect organs from ischemic damage is to restore proteome integrity, which could be achieved by boosting endogenous pathways central to proteostasis.^{3,4}

One major component of the cellular proteome resides in the endoplasmic reticulum (ER), the key organelle for biogenesis of the membrane and secretory proteins. Disruption of ER proteostasis leads to ER stress, which subsequently activates multiple

Correspondence to: Wei Yang, PhD, Department of Anesthesiology, Duke University Medical Center, Box 3094, 144 Sands Building, 303 Research Drive, Durham, NC 27710. E-mail: wei.yang@duke.edu

*Y. Shen and R. Li contributed equally.

Supplementary Material for this article is available at <https://www.ahajournals.org/doi/suppl/10.1161/JAHA.120.020216>

For Sources of Funding and Disclosures, see page 13.

© 2021 The Authors. Published on behalf of the American Heart Association, Inc., by Wiley. This is an open access article under the terms of the Creative Commons Attribution-NonCommercial-NoDerivs License, which permits use and distribution in any medium, provided the original work is properly cited, the use is non-commercial and no modifications or adaptations are made.

JAHA is available at: www.ahajournals.org/journal/jaha

CLINICAL PERSPECTIVE

What Is New?

- Activation of ATF6 (activating transcription factor 6) signaling in neurons is prosurvival and improves functional outcome after cardiac arrest and resuscitation.
- ATF6-mediated beneficial effects are associated with enhanced cellular capacity to restore protein homeostasis disrupted by ischemia/reperfusion insult after cardiac arrest and resuscitation.
- Cardiac arrest outcome is significantly improved by a pharmacologic treatment with compound 147, a selective ATF6 pathway activator.

What Are the Clinical Implications?

- Targeting the ATF6 pathway may represent a promising proteostasis-based therapeutic strategy to ameliorate ischemia/reperfusion injury after cardiac arrest and resuscitation.

Nonstandard Abbreviations and Acronyms

ATF6	activating transcription factor 6
CA	cardiac arrest
DEG	differentially expressed gene
ER	endoplasmic reticulum
ERAD	endoplasmic reticulum-associated degradation
FJC	fluoro-Jade C
GRP78	glucose-related protein 78
IRE1	inositol-requiring enzyme 1
PERK	protein kinase RNA-like endoplasmic reticulum kinase
RNA-Seq	RNA sequencing
sATF6	short-form activating transcription factor 6
UPR	unfolded protein response
XBP1	X-box binding protein-1

adaptive stress response pathways, collectively known as the unfolded protein response (UPR).⁵ The UPR has 3 major branches, named after 3 ER stress sensor proteins: ATF6 α (activating transcription factor 6 α ; hereafter referred to as ATF6), IRE1 (inositol-requiring enzyme 1), and PERK (protein kinase RNA-like ER kinase). Activation of these 3 UPR branches reshapes a large network of signaling pathways via translational and transcriptional reprogramming of many cellular processes such as protein folding, protein degradation, and cellular redox maintenance. Specifically, upon

activation, PERK phosphorylates eukaryotic initiation factor 2 α , which suppresses global protein translation, thus decreasing the ER workload. Activation of the ATF6 and IRE1 branches generates 2 transcriptional factors: sATF6 (short-form ATF6, produced by cleavage of ATF6 in the Golgi) and XBP1s (spliced X-box binding protein-1). Both transcriptional factors can upregulate expression of the same and also different genes that include genes encoding for ER chaperones (eg, GRP78 [glucose-related protein 78]), folding enzymes (eg, PDI [protein disulfide isomerase]), and ERAD (ER-associated degradation) proteins (eg, Derlin).^{6,7} Of note, ERAD is a major cellular degradation pathway, which is responsible for clearing potentially toxic terminally misfolded proteins that accumulate in the ER under physiologic and pathologic states.⁸ Thus, the ATF6 and IRE1 branches respond to ER stress by enhancing ER capacity to correctly fold proteins and clear the unfolded/misfolded proteins in the ER.

In general, among the 3 UPR branches, the ATF6 branch has been the least studied, possibly because of lack of an obvious phenotype manifested in *Atf6a* null mice. It has been shown that global deletion of *Xbp1* is embryonic lethal in mice, and *Perk* null mice exhibit severe postnatal growth retardation, indicating their critical roles in organismal development.^{9,10} By contrast, *Atf6a* null mice do not show any prominent phenotype,⁷ suggesting its nonessential role in healthy mice. However, accumulating evidence suggests that the ATF6 UPR branch is required for the full upregulation of UPR target genes, thus optimizing ER stress-related UPR activation, and is believed to play a primary role in pathologic states by facilitating restoration of cellular homeostasis.⁷ ATF6 deficiency renders organs more vulnerable to ischemic stress, because it has been shown that *Atf6a* null mice have a worse outcome after myocardial ischemia or brain ischemia.^{11,12} The ATF6 UPR branch is an emerging prosurvival pathway that shows great therapeutic potential for ischemia-related diseases.⁴

Cardiac arrest (CA) followed by resuscitation represents probably the most extreme scenario of ischemia/reperfusion injury for humans. Brain damage is a major pathologic consequence of CA that can lead to long-term neurologic disability or even death. It has been well established that CA causes ER stress, and activates the UPR in various organs including the brain.^{5,13,14} However, unlike the PERK and IRE1 UPR branches, the ATF6 branch appears to not be activated in the postischemic brain,¹³⁻¹⁵ which may confer brain cells less resistant to proteotoxic stress caused by ischemic insult. Notably, the ATF6 branch has been extensively studied in the heart. Several studies have demonstrated that this pathway plays a critical role in protein quality control in the heart, and boosting it exerts marked protection against heart ischemia and hypertrophy.^{4,16-18} However, its role in CA remains

undefined. Thus, motivated by previous promising findings, we designed the current study to investigate effects of activation of the ATF6 UPR branch in CA.

To determine the effects on CA outcome of activating the ATF6 branch in the brain, we took advantage of our conditional and inducible sATF6-KI (sATF6 knock-in) mouse line.¹⁵ We first demonstrated that compared with control mice, sATF6-KI mice with neuron-specific activation of the ATF6 UPR branch exhibited significantly better CA outcome. We then performed RNA sequencing (RNA-Seq) analysis on sATF6-KI hippocampal tissues, and obtained the first data set of the transcriptome regulated by the ATF6 branch in the brain. The RNA-Seq data revealed that many ERAD-related genes were upregulated by sATF6 in neurons. Consistent with this finding, CA-induced K48-linkage polyubiquitination was significantly higher in sATF6-KI mouse brains compared with controls. Finally, we treated mice with a newly identified ATF6 activator, the small molecule 147, and found that compound 147-treated mice showed significantly improved CA outcome. Together, our data indicate that the ATF6 UPR branch is a prosurvival pathway and may be considered as a therapeutic target for CA.

METHODS

The data that support the findings of this study are available from the corresponding author upon reasonable request. The protocols for all experiments conducted in this study were approved by the Institutional Animal Care and Use Committee at Duke University. Because this study focused on a conserved response pathway, only male sex was used. However, we cannot exclude the potential sex-specific effect in our study. For future preclinical studies on this pathway, female mice should be included. The online tool Quickcalcs (GraphPad Software, San Diego, CA) was used to randomize animals for group assignments. All outcome assessments were conducted by experimenters who were blinded to genotypes and group assignments. Information for the animals used in all outcome experiments is summarized in Table S1.

Animals

C57Bl/6 mice were obtained from The Jackson Laboratory (Bar Harbor, ME). The Cre-dependent and tamoxifen-inducible sATF6 knock-in mouse line, Rosa26-sATF6-MER, was generated previously in our laboratory.¹⁵ Of note, the gene segment of sATF6 is tagged with the FLAG at the N-terminus, and is also fused to the mutated estrogen receptor (MER) at the C-terminus. Because of MER presence, the fusion protein sATF6-MER is retained in the cytosol. Tamoxifen treatment can trigger the translocation of sATF6-MER

to the nucleus, where ATF6-dependent gene expression is then induced, thereby activating the ATF6 UPR branch. To express sATF6 in neurons, Rosa26-sATF6-MER was cross-bred with Emx1-Cre mice (Jackson Laboratory 005628) to generate Rosa26-sATF6-MER; Emx1-Cre (sATF6-KI) mice. Littermate Emx1-Cre mice were used as controls. The mouse line sATF6-KI has been extensively characterized previously.¹⁵ In total, this study used 84 mice, including 21 C57Bl/6, 30 sATF6-KI, and 33 littermate control mice.

CA and Cardiopulmonary Resuscitation Surgery

CA/cardiopulmonary resuscitation (CPR) surgery was performed as described previously.^{13,19} Briefly, anesthesia was induced with 5% isoflurane. After endotracheal intubation, mice were maintained on 1.5% to 1.7% isoflurane before CA induction. Body temperature was measured with a rectal temperature probe and maintained at $36.8 \pm 0.2^\circ\text{C}$ before CA. An ECG was continuously recorded. KCl (30 μL of 0.5 mol/L) was infused to induce asystole, which was verified by ECG and an absence of spontaneous respiration. Immediately after CA onset, mechanical ventilation was terminated, and pericranial temperature was maintained at $38.5 \pm 0.2^\circ\text{C}$ while allowing body temperature to drop during CA. At 8.5 minutes after CA, mechanical ventilation with 100% oxygen was resumed, and a bolus of epinephrine (100 μL of 32 $\mu\text{g}/\text{mL}$) was given, followed by continuous infusion (25 $\mu\text{L}/\text{min}$) accompanied by rapid chest compression using a single finger. Return of spontaneous circulation was established by appearance of stable ECG sinus rhythms. If return of spontaneous circulation was not achieved within 3 minutes, resuscitation was abandoned, and the animal was excluded from the study. When spontaneous respiration was adequate, mice were returned to their home cages. Sham-operated mice were subjected to the same surgical procedures until the jugular vein was exposed. Mice were then kept under isoflurane with mechanical ventilation for 15 minutes, allowing comparable exposures of sham and CA/CPR mice to isoflurane anesthesia.

Drug Administrations

Tamoxifen (Cayman; No. 13258; 20 mg/mL) was suspended in corn oil (Sigma; No. C8267). Animals were treated with 100 mg/kg tamoxifen or corn oil (vehicle) by oral gavage once daily for 5 days. Compound 147 (Tocris Bioscience; No. 6759) was suspended in 10% dimethyl sulfoxide (Sigma; No. D2650). Mice were administered compound 147 (2 mg/kg) or vehicle (10% dimethyl sulfoxide) via the tail vein 24 hours before surgery and 30 minutes after return of spontaneous circulation.

Behavioral Tests

All tests were conducted in the light phase, and the procedures were essentially the same as described previously.^{13,19–21} Briefly, a 9-point scoring system was used to evaluate general functional deficits (9 points=normal, and 0 points=severe injury).²⁰ The duration that each mouse was able to remain on the vertical screen, horizontal rod, and horizontal rope was recorded and then a score was assigned (0–3 points for each test). The rotarod test evaluated balance, grip strength, and motor coordination using a device with an accelerating rotating rod (4–40 rpm; Med Associates). Animals were trained for 3 days before the surgery to ensure a similar baseline. Latency to fall (average of 3 trials) was recorded. The open field test assessed general health status. The animal was placed in an open field box (50×50×50 cm; CleverSys, Reston, VA), and allowed to move freely while being video recorded. The video data were then analyzed by the automated tracking system TopScan (CleverSys). The total distance traveled during the 10-minute period of the test was calculated.

Histology

Mice were anesthetized and transcardially perfused with saline, followed by 4% paraformaldehyde. Frozen brain sections (20- μ m thick) were used for Fluoro-Jade C (FJC) staining to identify neuronal cell death.¹³ Briefly, the slices were incubated in 0.06% potassium permanganate for 10 minutes, and then immersed in FJC staining solution (Millipore; No. AG325) for 30 minutes. Sections were imaged using a fluorescence microscope. An evaluator, who was blinded to experimental groups, counted FJC-positive cells in both entire hippocampi of each brain section (around bregma –2.06 mm). Data are presented as a mean of total FJC-positive cells (2 hippocampi) for each mouse.

Quantitative Reverse Transcription–Polymerase Chain Reaction

The mRNA levels of selected genes were analyzed by quantitative reverse transcription–polymerase chain reaction. In short, total RNA was extracted from brain hippocampus samples using TRIzol reagent (ThermoFisher; No. 15596026), followed by cDNA synthesis (ThermoFisher; No. 18091050). Quantitative reverse transcription–polymerase chain reaction was performed using a Lightcycler 2.0 (Roche, Mannheim, Germany). All primers used in this study are listed in Table S2.

RNA-Seq Analysis

For the RNA-Seq analysis, total RNA was first prepared using TRIzol, and then treated with DNase I,

followed by purification using the RNeasy MinElute Cleanup kit (Qiagen; No. 74204). The integrity and concentration of the RNA samples were evaluated in an Agilent Bioanalyzer (Agilent Technologies, Santa Clara, CA) and Qubit 2.0 (ThermoFisher), respectively. RNA-Seq analysis was performed in the Genomic Analysis and Bioinformatics Shared Resource at Duke University Medical Center, similarly to our previous study.²² Briefly, total RNA (500 ng/sample) was used for library construction with the KAPA Stranded mRNA-Seq Kit (Kapa BioSystems, Wilmington, MA). Sequencing was performed on the Illumina HiSeq 4000 sequencing platform and de-multiplexed using bcl2fastq2 v2.20. The raw sequencing data are available in the Gene Expression Omnibus database (National Institutes of Health, National Library of Medicine, Bethesda, MD; accession number GSE160259). For data analysis, we first cleaned up low-quality bases and sequencing adapters with the TrimGalore toolkit, and then mapped reads to the GRCh38v68 version of the mouse genome and transcriptome using the STAR RNA-Seq alignment tool. Gene counts were quantified using the HTSeq tool, and normalization and differential expression were analyzed using the DESeq2 Bioconductor package with the R (R Foundation for Statistical Computing, Vienna, Austria) statistical programming environment. The false discovery rate (shown as *P*adj) was calculated to control for multiple hypothesis testing. For the heatmap, gene expression has been z-score normalized, and the samples and genes are clustered by correlation distance with complete linkage. A gene ontology category database was applied for biological process, molecular function, and cellular component annotation of differentially expressed genes (DEGs). Enrichment analysis of gene ontology categories was performed using DAVID online tools (<https://david.ncifcrf.gov>). The Ingenuity Pathway Analysis (Ingenuity Systems, Redwood City, CA) online program was used to identify function and canonical pathways.

Western Blotting

Tissue samples were processed using our standard method.¹³ Briefly, the brain hippocampus was dissected on ice and snap frozen in liquid nitrogen as quickly as possible to prevent deconjugation of ubiquitinated proteins. Tissue samples were homogenized by sonication using lysis buffer supplemented with 2% SDS. Protein samples were run on 4% to 12% Bis-Tris Plus gels (ThermoFisher), and were transferred to polyvinylidene difluoride (PVDF) membranes. After blocking, membranes were incubated with a primary antibody at 4°C overnight. After extensive washing, membranes were incubated with a secondary antibody for 1 hour at room temperature. Proteins were

then detected with the enhanced chemiluminescence (ECL) analysis system (GE Healthcare). Quantification of signal intensities was performed using ImageJ (National Institutes of Health). The primary antibodies are listed in Table S3.

Statistical Analysis

Sample sizes were determined based on our previous studies using the same CA/CPR model. Data were analyzed using Prism 8 software (GraphPad, LaJolla, CA). Statistical analysis was assessed by Mann-Whitney *U* test for neurologic scores, Mantel-Cox log-rank test for survival rates, unpaired Student *t* test for 2 groups, and 1-way ANOVA with post hoc Fisher least significant difference test for >2 groups. Data are presented as mean±SEM, median, or percentage. For RNA-Seq analysis, selection of DEGs was based on adjusted *P*<0.05 with fold change >1.5 or <-1.5. For other analyses, the level of significance was set at *P*<0.05.

RESULTS

CA Outcome Was Improved After Neuron-Specific Activation of the ATF6 UPR Branch

We previously generated a conditional and tamoxifen-inducible sATF6 knock-in mouse line, which is a valuable tool particularly for studying the ATF6 UPR branch in various cell types.¹⁵ Here, to clarify the effect of activating the ATF6 branch in neurons after CA/CPR, we used sATF6-KI mice, in which transgene sATF6 is expressed predominantly in forebrain neurons. First, both control and sATF6-KI mice received tamoxifen dosing for 5 days to induce the nuclear translocation of sATF6 and thus activate downstream ATF6 signaling in sATF6-KI mice. After 3 days of recovery to clear tamoxifen, mice were subjected to 8.5 minutes CA using our CA/CPR model. Compared with control mice, sATF6-KI mice appeared to require less CPR time (Figure 1A). Also, sATF6-KI mice trended toward less body weight loss on day 3 after CA/CPR (Figure 1B).

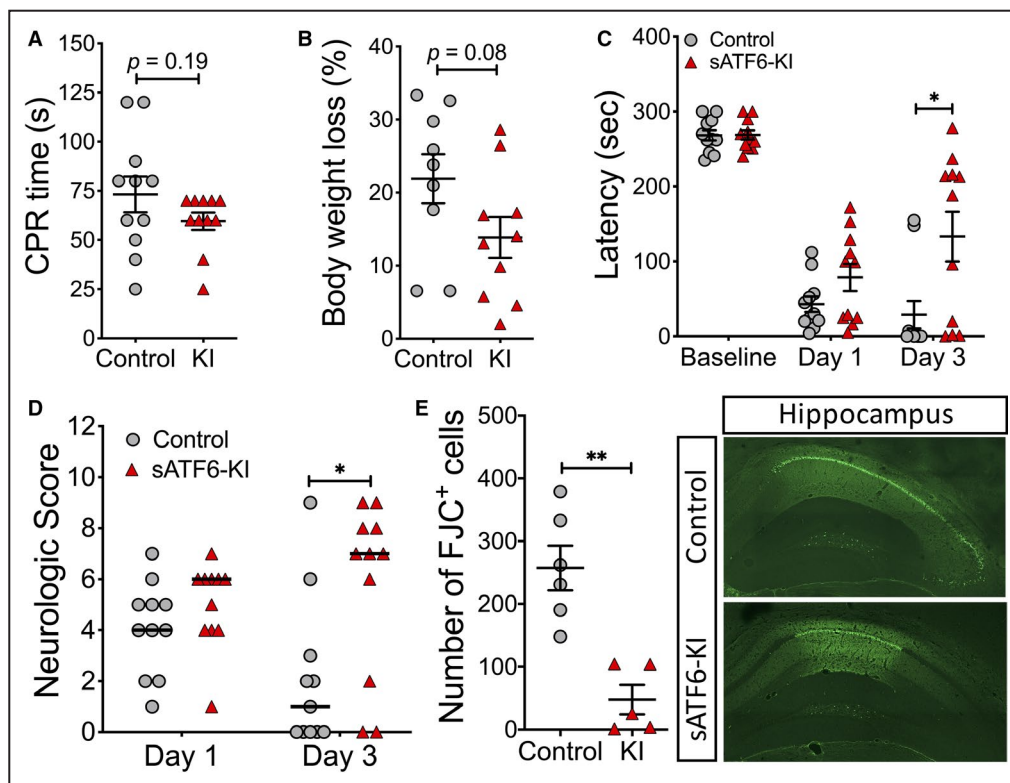


Figure 1. Cardiac arrest (CA) outcome was improved after neuron-specific activation of the ATF6 (activating transcription factor 6) unfolded protein response branch.

Littermate control and short-form ATF6 knock-in (sATF6-KI [KI]) mice were treated with tamoxifen for 5 days. Three days later, mice (n=11–12/group) were subjected to 8.5 minutes CA. **A**, Cardiopulmonary resuscitation (CPR) time. **B**, Body weight loss on day 3 after CA/CPR. **C**, Rotarod test. **D**, Neurologic scores. Of note, dead mice (2 in control group and 1 in KI group) were also shown in the figure (score=0), but were excluded from statistical analysis. **E**, Neuronal death in the hippocampus after CA/CPR. On day 3 after CA/CPR, brain sections were stained with Fluoro-Jade C (FJC). The number of FJC-positive neurons in the hippocampus was counted (n=5–6/group). Representative images are shown on the right. Data are presented as median or mean±SEM. **P*<0.05. ***P*<0.01.

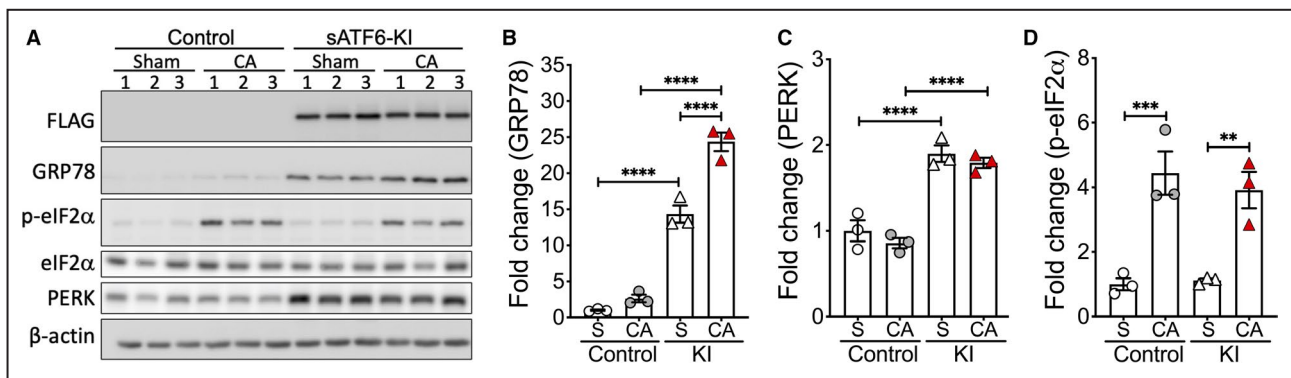


Figure 2. Activation of the PERK (protein kinase RNA-like ER kinase) unfolded protein response branch after cardiac arrest/cardiopulmonary resuscitation (CA/CPR) was similar between control and sATF6-KI (short-form activating transcription factor 6 knock-in) mice.

Both control and sATF6-KI (KI) mice were subjected to sham (S) or CA/CPR surgery. Brain hippocampus samples were collected at 3 hours after CA/CPR. Levels of sATF6 (FLAG), GRP78 (glucose-related protein 78), p-eIF2 α (phosphorylated eukaryotic initiation factor 2 α), and PERK were evaluated by Western blotting (A). Quantification data are shown for GRP78 (B), PERK (C), and p-eIF2 α (D). β -actin was used as a loading control. The mean values in control sham samples were set to 1.0. Data are presented as mean \pm SEM. ** P <0.01. *** P <0.001. **** P <0.0001.

To evaluate functional recovery, rotarod test and neurologic scoring were performed on day 1 and day 3 after CA/CPR. On day 1 after CA/CPR, sATF6-KI mice tended to perform better in both tests compared with control mice, and this improvement reached statistical significance on day 3 (Figure 1C and 1D). Finally, we examined neuronal death in the hippocampus on day 3 after CA/CPR using FJC staining. Consistent with behavioral results, sATF6-KI mice had significantly fewer FJC-positive cells, indicating more surviving neurons after CA/CPR (Figure 1E). Based on these data, we then attempted to determine the extent to which sATF6-KI mice exhibited improved long-term outcome (ie, 14 days after CA/CPR) (Figure S1). However, this experiment suffered a high mortality rate in the control group versus sATF6-KI group (55.6% versus 14.3% on day 14 after CA, respectively), which confounded long-term functional assessments. However, even considering the potential survival bias and the small mouse number in the control group, sATF6-KI mice appeared to have a better outcome than control mice (Figure S1). Collectively, our data indicate that activation of the ATF6 branch in neurons was sufficient to

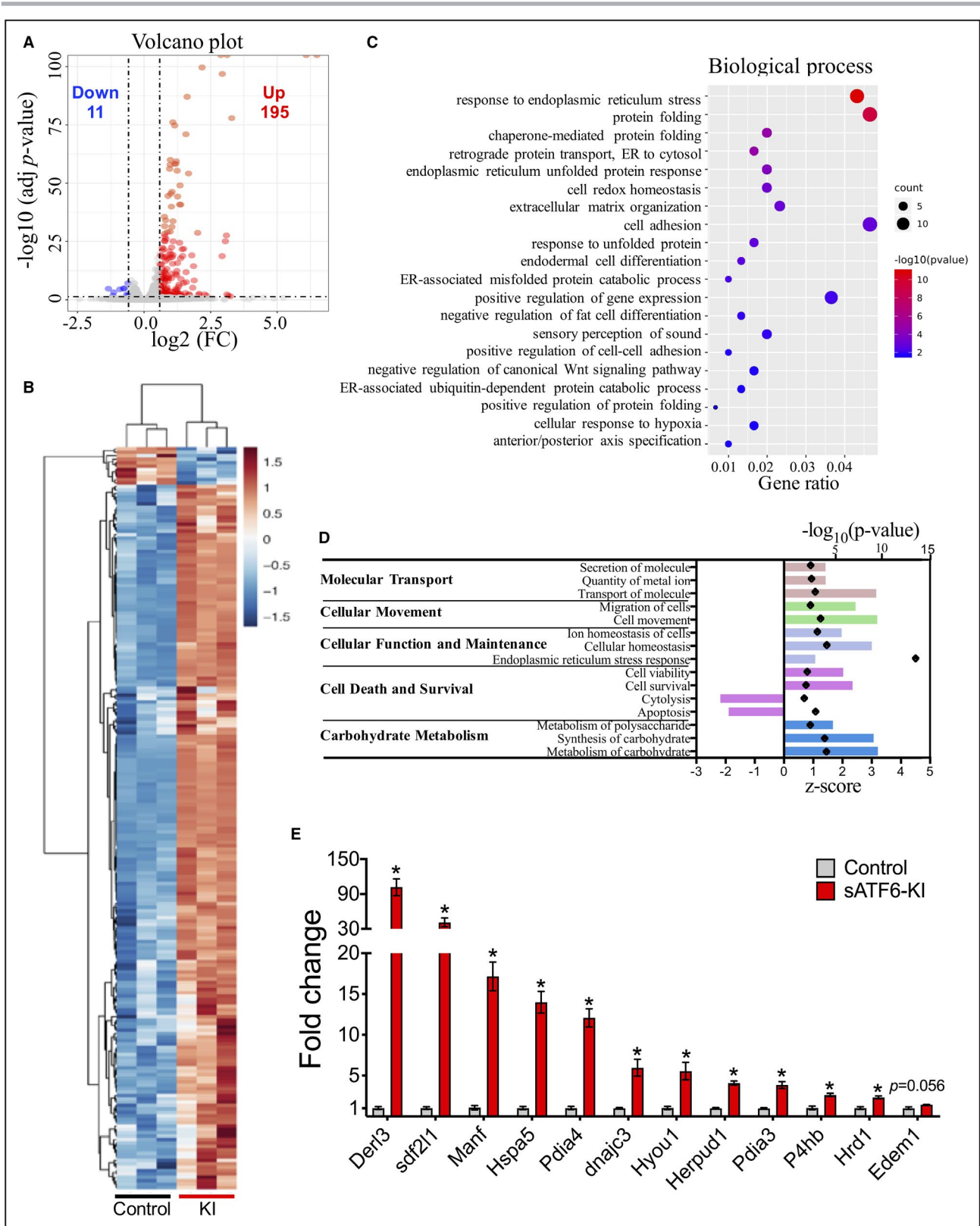
reduce neuronal injury and improve functional recovery after CA/CPR.

Pro-Proteostatic Genes, Many Related to the ERAD Pathway, Were Upregulated After Neuron-Specific Activation of the ATF6 UPR Branch

As the first step toward understanding the mechanisms responsible for improved CA outcome in sATF6-KI mice, we examined another UPR pathway (ie, the PERK branch) using eukaryotic initiation factor 2 α phosphorylation as an indicator. As expected, GRP78 protein levels were considerably higher in sATF6-KI mice, compared with control mice (Figure 2). Interestingly, PERK protein levels were also significantly increased in the sATF6-KI mouse brains. However, levels of CA-induced eukaryotic initiation factor 2 α phosphorylation were not different between control and sATF6-KI mice (Figure 2), suggesting a similar activation of the PERK branch. This result is consistent with our previous finding in an ischemic stroke model.¹⁵ Next, considering that sATF6 is a transcriptional factor, we speculated that the protective effects of the ATF6

Figure 3. RNA sequencing (RNA-Seq) analysis.

Hippocampus samples from control and sATF6-KI (short-form activating transcription factor 6 knock-in [KI]) mice were analyzed by RNA-Seq. A, Volcano plot. This plot depicts distribution of significance ($-\log_{10}$ [adjusted {adj} P value]) vs fold change (FC) (\log_2 [fold change]) for all genes. The blue dots indicate downregulated genes (FC < -1.5, adj P < 0.05), the red dots indicate upregulated genes (FC > 1.5, adj P < 0.05), and the gray dots indicate genes with no significant change. Horizontal dashed lines indicate adj P value of 0.05. Vertical dashed lines indicate expression fold change equal to 1.5 and -1.5, respectively. B, Heatmap plot of differentially expressed genes (DEGs) between control and sATF6-KI mice. C, Top 20 overrepresented gene ontology (GO) biological processes of DEGs. The size and color of the circle indicate the number and $-\log_{10}$ (P value) of DEGs annotated in the specific GO biological processes, respectively. D, Enrichment functional analysis with Ingenuity Pathway Analysis. Top enriched functions were clustered into 5 groups. The bars indicate z score, with >2 for activation and <-2 for inhibition. The black diamonds indicate statistical significance ($-\log_{10}$ [P -value]) for each term. E, Quantitative polymerase chain reactions validation of selected DEGs from RNA-Seq analysis. Data are presented as mean \pm SEM (n=3/group). * P <0.05. ER indicates endoplasmic reticulum.



UPR branch may be because of prosurvival genes and related processes upregulated by sATF6. However, no study has yet systematically analyzed ATF6-regulated genes in the brain. Thus, we performed an

RNA-Seq analysis to characterize the gene expression profile in the sATF6-KI mouse brain (Figure 3). Hippocampus tissue samples were collected from control and sATF6-KI mice on day 3 after 5 days of

Table 1. Top Differentially Expressed Genes (sATF6-KI Versus Control Mice)

Gene Symbol	Gene Name	Fold Change	P_{adj} Value
Upregulated			
<i>Derl3</i>	Derlin 3	89.88	<0.001
<i>Esr1</i>	Estrogen receptor 1	67.99	<0.001
<i>Sdf2l1</i>	Stromal cell-derived factor 2 like 1	12.93	<0.001
<i>Tes</i>	Testin LIM domain protein	9.79	<0.001
<i>Gckr</i>	Glucokinase regulator	8.64	0.005
<i>Acsm4</i>	Acyl-CoA synthetase medium chain family member 4	8.94	0.020
<i>Manf</i>	Mesencephalic astrocyte-derived neurotrophic factor	8.66	<0.001
<i>Trh</i>	Thyrotropin-releasing hormone	8.52	<0.001
<i>Scarf2</i>	Scavenger receptor class F member 2	8.18	<0.001
<i>Fkbp11</i>	FKBP prolyl isomerase 11	7.61	<0.001
<i>C1qtnf1</i>	C1q and tumor necrosis factor-related protein 1	7.64	<0.001
<i>Rbm15b</i>	RNA binding motif protein 15B	7.37	<0.001
<i>Pdia4</i>	Protein disulfide isomerase family A member 4	7.36	<0.001
<i>Hspa5</i>	Heat shock protein family A member 5	5.41	<0.001
<i>Gnb3</i>	G protein subunit beta 3	5.08	0.018
Downregulated			
<i>Inhba</i>	Inhibin beta A chain	-1.52	0.028
<i>Syce2</i>	Synaptonemal complex central element protein 2	-1.52	0.017
<i>Homer3</i>	Homer scaffolding protein 3	-1.52	<0.001
<i>Mc4r</i>	Melanocortin 4 receptor	-1.55	0.024
<i>Gm129</i>	Circadian-associated repressor of transcription	-1.57	0.005
<i>Prss35</i>	Serine protease 35	-1.67	<0.001
<i>Lefty1</i>	Left-right determination factor 1	-1.71	<0.001
<i>Alox12b</i>	Arachidonate 12-lipoxygenase, 12R type	-1.88	<0.001
<i>Col6a4</i>	Collagen, type VI, alpha 4	-2.20	<0.001
<i>Scgn</i>	Secretagogin, EF-hand calcium binding protein	-2.25	0.020
<i>Asb11</i>	Ankyrin repeat and SOCS box containing 11	-2.53	<0.001

sATF6-KI indicates short-form activating transcription factor 6 knock-in.

tamoxifen administration. The volcano plot showed that most of the DEGs were upregulated in sATF6-KI brains (Figure 3A). After filtering the data with our selection criteria (fold change >1.5 or <-1.5; P_{adj} <0.05), we found that 195 genes were upregulated, and only 11 genes were downregulated (Figure 3A and 3B). We have listed the top DEGs (top 15 from upregulated genes and all 11 downregulated genes) in Table. Then, we subjected DEGs to gene ontology analysis and Ingenuity Pathway Analysis (Figure 3C and 3D and Figure S2). As expected, enriched biological processes, as well as the cell component and molecular function, were primarily associated with adaptive ER stress response, protein folding and degradation, and redox homeostasis (Figure 3C, Figure S2A). Consistently, the Ingenuity Pathway Analysis identified 4 activated pathways including the unfolded protein response, ER stress pathway, GP6 (glycoprotein 6) signaling pathway, and NRF2 (nuclear factor erythroid 2-related factor 2)-mediated oxidative stress

response (z score >2) (Figure S2B). Further analysis indicated that significantly upregulated function categories are associated with molecular transport, cell movement, cell function and maintenance, cell death/survival, and carbohydrate metabolism (Figure 3D). Interestingly, increased functions (indicated by positive z scores) include transport of molecule, cellular homeostasis, and cell survival, whereas decreased functions (indicated by negative z scores) are associated with cytolysis and apoptosis (Figure 3D). Notably, at least 9 ERAD core components (P_{adj} <0.001) were upregulated (Table S4).²³ Among the DEGs, the most upregulated gene was Derlin 3 (*Derl3*), a key component of the ERAD machinery.^{24,25} Using quantitative reverse transcription-polymerase chain reaction, we confirmed significant upregulation of 4 ERAD core genes (*Derl3*, *Hspa5*, *Herpud1*, and *Hrd1*) as well as 7 other genes from the list of DEGs (Figure 3E).

To further verify an increase in ERAD components in sATF6-KI versus control mouse brains, we performed

Western blotting analysis in CA samples. Control and sATF6-KI mice were subjected to sham or CA/CPR surgery, and at 3 hours reperfusion, hippocampus samples were collected and analyzed. Compared with control mice, sATF6-KI mice showed significantly higher levels of Sel1l (sel-1 suppressor of lin-12-like), OS9 (osteosarcoma amplified 9), VCP (valosin-containing protein), and HERP (or Herpud1; Homocysteine-inducible endoplasmic reticulum stress-inducible ubiquitin-like domain member 1). However, at this time point of reperfusion, CA/CPR itself appeared to have no significant effect on the protein levels of any of these ERAD components (control groups; Figure 4). Notably, previous studies have suggested that improving ERAD capacity by upregulating related genes markedly protects the heart from ischemic insult.^{24,26}

In addition, from the RNA-Seq data, we also noted that mesencephalic astrocyte-derived neurotrophic factor (MANF) was significantly upregulated in sATF6-KI mouse brains, which was validated by qRT-PCR (Figure 3E). Because MANF is a potent neuroprotective molecule, we assessed MANF protein levels, and confirmed its increase in sATF6-KI mice

(Figure 4G). Taken together, data indicate that the ERAD machinery as a whole is boosted by activation of the ATF6 UPR branch. It is reasonable to suggest that augmented ERAD capacity to clear misfolded proteins and thus resolve perturbed ER proteostasis in neurons contributes to the improved CA outcome observed in sATF6-KI mice.

Protein Ubiquitination Was Differentially Increased in Control and sATF6-KI Mouse Brains After CA/CPR

Based on the data above, the next step would be to confirm an increase in ERAD activity in sATF6-KI mouse brains after CA/CPR. However, because no universal or brain-specific ERAD substrate has been identified, an established way to directly measure ERAD activity in vivo in the brain is not yet available. Alternatively, we analyzed ubiquitination levels in the post-CA brain because ubiquitination is a key step in the ERAD pathway. We speculated that if sATF6-expressing neurons can more efficiently label unwanted proteins for degradation via the ERAD

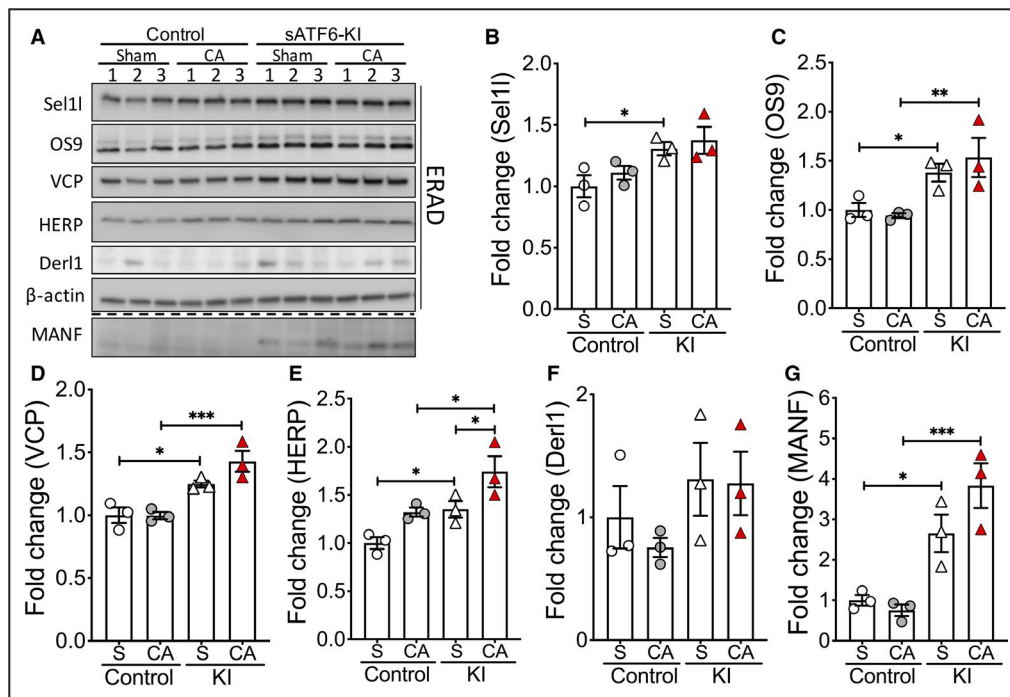


Figure 4. Endoplasmic reticulum-associated degradation (ERAD) pathway in sATF6-KI (short-form activating transcription factor 6 knock-in) mice.

Control and sATF6-KI (KI) mice were subjected to sham (S) or cardiac arrest/cardiopulmonary resuscitation (CA/CPR) surgery. Brain hippocampus samples were collected at 3 hours after CA/CPR. **A**, Levels of core ERAD components were evaluated by Western blotting. Quantification of protein expression is shown for Sel1l (sel-1 suppressor of lin-12-like; **B**), OS9 (osteosarcoma amplified 9; **C**), VCP (valosin-containing protein; **D**), HERP (homocysteine-inducible ER stress protein; **E**), and Der1l (derlin-1; **F**). Additionally, another endoplasmic reticulum stress-related protein MANF (mesencephalic astrocyte-derived neurotrophic factor) was examined (**G**). Protein levels were normalized to β -actin. The mean values from control sham samples were set to 1.0. Data are presented as mean \pm SEM ($n=3$ /group). * $P<0.05$. ** $P<0.01$. *** $P<0.001$.

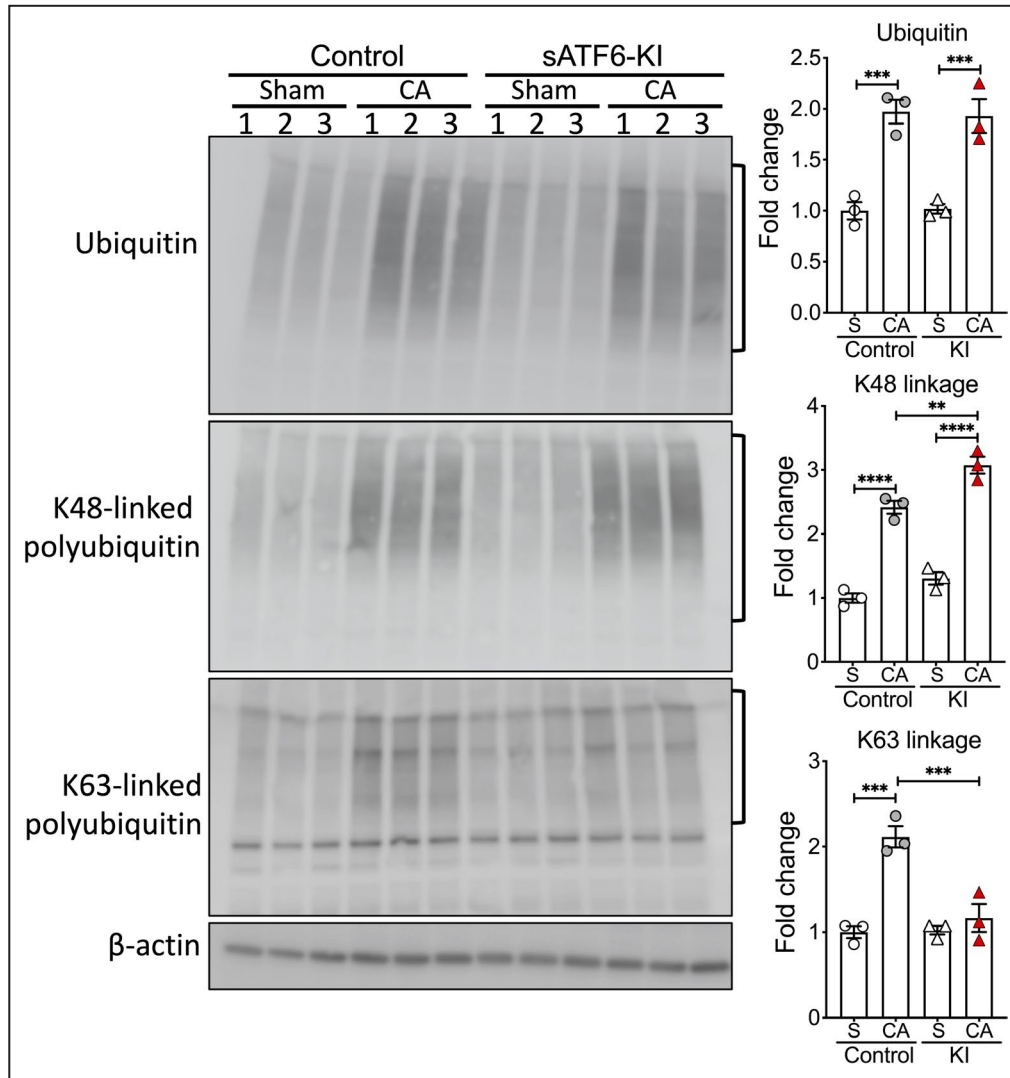


Figure 5. Ubiquitination in sATF6-KI (short-form activating transcription factor 6 knock-in) mice. Both control and sATF6-KI (KI) mice were subjected to sham (S) or cardiac arrest/cardiopulmonary resuscitation (CA/CPR) surgery. Brain hippocampus samples were collected at 3 hours after CA/CPR. Levels of global ubiquitin, K48-linked polyubiquitin, and K63-linked polyubiquitin were evaluated by Western blotting. The high molecular-weight regions, marked by brackets, were used for quantification of ubiquitination. β -actin was used as a loading control. The mean values in control sham samples were set to 1.0. Data are presented as mean \pm SEM (n=3/group). ** P <0.01. *** P <0.001. **** P <0.0001.

pathway, the level of proteins that are ubiquitinated for degradation would be higher in sATF6-KI mice than in control mice. To test this, we measured ubiquitination levels in the post-CA brain (Figure 5). Consistent with our previous reports,^{13,27,28} levels of global ubiquitination were robustly increased after CA/CPR, although to a similar extent in control and sATF6-KI mice. Of note, ubiquitination regulates different biological processes according to the linkage types of which K48- and K63-linkages have been commonly examined.²⁹ Especially, K48-linked polyubiquitin chains serve as the principal linkage signal for protein degradation. Thus, we further examined the changes of these 2 polyubiquitin linkages. Interestingly, the increase

in K48-linked polyubiquitin chains was significantly higher in sATF6-KI versus control mice, whereas the K63-linkage signal was significantly lower in sATF6-KI mice (Figure 5).

CA Outcome Was Improved in Mice Treated With Compound 147

Finally, we set out to determine whether pharmacologic activation of the ATF6 branch improves CA outcome. To this end, we tested the compound 147. Compound 147 was among the first small molecules identified as specific ATF6 activators through phenotypic screening.³⁰ A previous time-course experiment indicates

that induction of ATF6-regulated genes reaches a maximum at 24 hours after compound 147 administration.¹⁶ Thus, as the first attempt of testing compound 147 in CA, we chose a dosing regimen similar to one used in the recent study¹⁶ (ie, pretreatment at 24 hours before CA/CPR surgery plus post-treatment at 30 minutes after return of spontaneous circulation). We had 2 experimental groups: CA+vehicle and CA+compound 147. There was no significant difference in CPR time between the 2 groups (Figure 6A). On day 3 after CA/CPR, however, we found that mice treated with compound 147 performed significantly better in both neurologic scoring and the open field test (Figure 6B and 6C). Moreover, the survival rate over 3 days following CA was significantly improved after compound 147 treatment (Figure 6D).

DISCUSSION

Here, we present our results of the first experimental study designed to determine the role of the ATF6 UPR branch in CA outcome. Using genetic and pharmacologic approaches, we provide evidence that the ATF6 UPR branch is a pro-survival pathway, and that its activation leads to significantly better CA outcome. Specifically, we found that forced activation of the ATF6 pathway in neurons was sufficient to improve functional recovery after CA/CPR. Such a protective effect is likely attributable to increased expression of many pro-proteostatic genes regulated by the ATF6, as revealed by our RNA-Seq analysis. The RNA-Seq data set generated in this study is also a valuable resource for understanding the role of the ATF6 UPR branch in neurons. Finally, we demonstrated that pharmacologically activating the ATF6 pathway with compound 147 is beneficial to CA outcome.

It is well established that ischemia/reperfusion leads to ER stress, and activates the UPR in various organs.⁵

However, the 3 UPR branches in the brain appear to respond differently to CA/CPR. Unlike cell culture studies in which all 3 UPR branches are normally activated in response to ER stress, activation of the PERK and IRE1 UPR branches in the post-CA brain is clearly evident, but such convincing evidence is lacking for the ATF6 UPR branch.^{13,14} For example, Kumar et al examined proteolysis of ATF6 in the post-CA brain, and did not find sATF6 (50 kDa) at 4 hours reperfusion after CA/CPR.¹⁴ However, there is a possibility that this failure to detect sATF6 in the post-CA brain is because when activated, sATF6 is rapidly degraded via the ubiquitin–proteasome system.³¹ Because upregulation of GRP78 is primarily controlled by the ATF6 branch,⁷ GRP78 protein levels could be also used as an indicator of ATF6 activation.¹² Thus, we evaluated GRP78 expression after CA/CPR, and observed a \approx 2-fold increase in GRP78 in the brain at 3 hours and at 24 hours reperfusion.¹³ This modest increase may suggest that the ATF6 branch is either not activated or only slightly activated in the brain early after CA/CPR. Given the accumulating evidence that an activated ATF6 branch is protective under various ischemia-related conditions,^{4,15,16} the lack of strong activation of this branch may partially be responsible for brain injury after CA/CPR. On the other hand, from a therapeutic point of view, the ATF6 branch may represent a promising target that can be further boosted for beneficial effects. In the current study, we showed that genetically boosting this branch in the brain improved CA outcome, a finding that is congruent with the therapeutic implication of targeting the ATF6 branch in ischemia-related diseases, which has been increasingly appreciated.⁴

Previous studies have revealed that activation the ATF6 pathway in the heart is protective because it can enhance the ERAD capacity and increase expression of ER chaperones to facilitate restoration of ER homeostasis.^{4,16–18} Our current data provide the first evidence

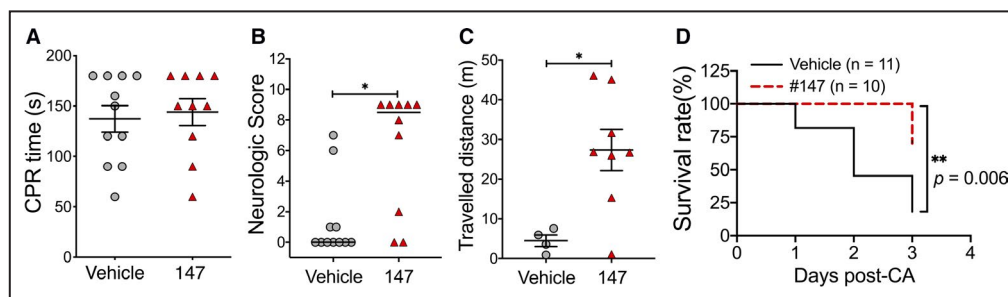


Figure 6. Cardiac arrest (CA) outcome was improved with compound 147 treatment.

C57Bl/6 mice were subjected to 8.5 minutes CA. Mice (n=10–11/group) received intravenous injection of compound 147 or vehicle 24 hours before CA/cardiopulmonary resuscitation (CPR) and 30 minutes after return of spontaneous circulation. Functional outcome and survival rates were evaluated on day 3 after CA/CPR. **A**, CPR time. **B**, Neurologic score. Of note, dead mice (7 in the vehicle group and 2 in the compound 147 group) were also shown in the figure (score=0) but were excluded from statistical analysis. **C**, Open field test. **D**, Survival rates. Of note, after the final behavioral tests, 1 mouse from the compound 147 group and 2 mice from the vehicle group died. Data are presented as median or mean \pm SEM. * P <0.05. ** P <0.01.

supporting that these mechanisms also underpin the beneficial effects of activated ATF6 pathway in the post-CA brain. Using RNA-Seq analysis, we found that most of the ATF6-regulated genes in the brain are related to ER stress, in particular, the ERAD pathway. The ERAD pathway essentially involves 4 processes: substrate recognition, substrate retro-translocation from the ER, ubiquitination, and proteasome-mediated degradation in the cytosol. In mammalian cells, many key components of the ERAD machinery have been identified. For example, substrate recognition involves GRP78, OS9, and EDEM (ER degradation-enhancing α -mannosidase-like), whereas HRD1, Sel1l, and HERP are essential components of a complex that plays a role in retro-translocation. HRD1 is also the major E3 ligase for ubiquitination of substrates and the degradation that follows with the help of VCP in the ERAD pathway. Moreover, a recent study attributes a crucial role to Der13 in forming the ERAD complex under ER stress.²⁵ Notably, many ERAD core components are significantly increased in neurons of sATF6-KI mice, according to our RNA-Seq analysis (Table S4). Thus, although ERAD function was initially proposed to be controlled by the IRE1/XBP1 pathway,³² our data and others support the notion that the ATF6 branch is a key regulator of ERAD.⁷ Only a few studies have examined the role of these ERAD components in ischemia/reperfusion injury. For example, *Der13* overexpression enhances clearance of misfolded protein in cultured cells, and protects cardiomyocytes from in vitro ischemia-induced cell death.²⁴ HERP knockout mice have significantly larger infarct volumes after cerebral ischemia.³³ Our data are consistent with these previous reports on the prosurvival effects of increased expression of ERAD components in ischemia/reperfusion injury.

In search of further support of a role for ERAD in the post-CA brain, we examined changes in ubiquitination after CA/CPR. If ERAD activity is enhanced in sATF6-KI mice, we would expect an increase in ubiquitinated proteins to be degraded in the post-CA brain. The functional consequence of ubiquitination is determined by how ubiquitin units are linked on target proteins. The most well-known polyubiquitin linkage occurs at K48. The K48-linkage is the principal signal for targeting proteins for degradation by the proteasome. Our previous proteomics study has revealed that the K48-linkage is the most upregulated polyubiquitin linkage after brain ischemia,²⁸ suggesting that the role of CA-induced ubiquitination is to eliminate dysfunctional proteins caused by perturbed proteostasis after ischemia. Because almost one third of total proteins are processed and matured in the ER, it is reasonable to speculate that a large portion of ubiquitinated proteins after brain ischemia are ER in origin, and that they are ubiquitinated via the ERAD pathway.

We examined both global and K48 ubiquitination in control and sATF6-KI mice after CA/CPR. Interestingly, although there was no difference in global ubiquitination between genotypes, sATF6-KI mice had significantly more K48-linkage polyubiquitination, which may indicate that the ERAD capacity was increased after activation of the ATF6 UPR branch. We also found that the CA-induced increase in the K63-linkage was significantly less in sATF6-KI mice. Because the K63-linkage has numerous functions,³⁴ the effect of this change on CA outcome remains to be determined.

In addition to ERAD components, we provided evidence that activation of ATF6 signaling induces expression of MANF in neurons. It has been shown that MANF is modestly increased after ischemia/reperfusion in various organs including the brain and heart.^{35,36} Notably, in a comprehensive preclinical study, the investigators injected viral vectors expressing transgene MANF into the peri-infarct region on day 2 after ischemic stroke, and found that overexpression of MANF significantly improves functional recovery. They also observed beneficial effects when recombinant MANF protein was delivered chronically into the ipsilesional hemisphere over 2 weeks after stroke. These data strongly support the therapeutic potential of MANF in brain ischemia.³⁷ The protective effects exerted by MANF may be attributed to its function as an ER-resident chaperone in maintaining protein-folding homeostasis.^{38,39} In our sATF6-KI mouse brains, MANF expression is markedly increased upon ATF6 activation, which likely contributes to the improved outcome. However, the extent of this contribution needs to be further clarified. To this end, the viral approach for in vivo gene silencing of MANF may be considered. Moreover, it is also appealing to conduct a preclinical study to examine the therapeutic potential of recombinant MANF protein treatment for CA.

Finally, we tested compound 147 in CA. Compound 147 is a small molecule that was identified via cell-based-reporter high-throughput screening,³⁰ and that selectively activates the ATF6 branch without considerable effects on the other 2 UPR branches. Recently, Blackwood et al extensively evaluated this compound in various disease models of ischemia/reperfusion injury.¹⁶ Their data indicate that compound 147 treatment robustly induces ATF6 target genes in the heart, and protects the heart from ischemia/reperfusion injury. Importantly, these protective effects of compound 147 were lost if *Atf6* was deleted in cardiomyocytes, confirming the specific function of compound 147 treatment. This study also showed that compound 147 treatment is beneficial in mouse models of renal ischemia/reperfusion injury and ischemic stroke. Such findings are particularly relevant to the current study because CA/CPR causes ischemia/reperfusion injury in all organs. We found that treatment with compound

147 significantly improves CA outcome. This improvement is likely a consequence of collective protective effects of compound 147 on various organs.

There are limitations in this study. It must be noted that in the experiments using sATF6-KI mice or compound 147 treatment, the ATF6 branch was already activated before CA, which represents a preconditioning scenario. The pretreatment to activate the ATF6 branch could be applicable in certain medical conditions, such as for patients undergoing cardiovascular surgeries that require a period of circulatory arrest. For out-of-hospital patients with cardiac arrest, however, only post-CA treatments are feasible. Thus, it remains to be determined whether post-CA activation of the ATF6 pathway also improves CA outcome. This is likely the case, based on the current evidence in heart ischemia and ischemic stroke.^{15,16} Moreover, to further examine the therapeutic potential of compound 147 in CA, future studies need to use both male and female, young and aged animals with long-term outcome evaluation including cognitive tests.

In summary, our data, together with a recent report,²¹ provide the first line of evidence that targeting the UPR may represent a promising proteostasis-based therapeutic strategy for ameliorating ischemia/reperfusion damage after CA.

ARTICLE INFORMATION

Received November 18, 2020; accepted April 21, 2021.

Affiliation

Department of Anesthesiology, Center for Perioperative Organ Protection, Duke University Medical Center, Durham, NC.

Acknowledgments

The authors thank P. Miao for her excellent technical support and K. Gage for her excellent editorial contribution.

Sources of Funding

This study was supported by funds from the Department of Anesthesiology (Duke University Medical Center), American Heart Association grants 16GRNT30270003 and 18CSA34080277, and National Institutes of Health grants NS099590 and NS097554.

Disclosures

None.

Supplementary Material

Tables S1–S4
Figures S1–S2

REFERENCES

- Labbadia J, Morimoto RI. The biology of proteostasis in aging and disease. *Annu Rev Biochem*. 2015;84:435–464. DOI: 10.1146/annurev-biochem-060614-033955.
- Gonzalez-Teuber V, Albert-Gasco H, Auyeung VC, Papa FR, Mallucci GR, Hetz C. Small molecules to improve or proteostasis in disease. *Trends Pharmacol Sci*. 2019;40:684–695. DOI: 10.1016/j.tips.2019.07.003.
- Wang ZR, Yang W. Impaired capacity to restore proteostasis in the aged brain after ischemia: implications for translational brain ischemia research. *Neurochem Int*. 2019;127:87–93. DOI: 10.1016/j.neuint.2018.12.018.
- Glembotski CC, Rosarda JD, Wiseman RL. Proteostasis and beyond: ATF6 in ischemic disease. *Trends Mol Med*. 2019;25:538–550. DOI: 10.1016/j.molmed.2019.03.005.
- Yang W, Paschen W. Unfolded protein response in brain ischemia: a timely update. *J Cereb Blood Flow Metab*. 2016;36:2044–2050. DOI: 10.1177/0271678X16674488.
- Shoulders MD, Ryno LM, Genereux JC, Moresco JJ, Tu PG, Wu C, Yates JR, Su AI, Kelly JW, Wiseman RL. Stress-independent activation of XBP1s and/or ATF6 reveals three functionally diverse er proteostasis environments. *Cell Rep*. 2013;3:1279–1292. DOI: 10.1016/j.celrep.2013.03.024.
- Wu J, Rutkowski DT, Dubois M, Swathirajan J, Saunders T, Wang J, Song B, Yau GD, Kaufman RJ. Atf6alpha optimizes long-term endoplasmic reticulum function to protect cells from chronic stress. *Dev Cell*. 2007;13:351–364. DOI: 10.1016/j.devcel.2007.07.005.
- Qi L, Tsai B, Arvan P. New insights into the physiological role of endoplasmic reticulum-associated degradation. *Trends Cell Biol*. 2017;27:430–440. DOI: 10.1016/j.tcb.2016.12.002.
- Zhang P, McGrath B, Li S, Frank A, Zambito F, Reinert J, Gannon M, Ma K, McNaughton K, Cavener DR. The PERK eukaryotic initiation factor 2 alpha kinase is required for the development of the skeletal system, postnatal growth, and the function and viability of the pancreas. *Mol Cell Biol*. 2002;22:3864–3874. DOI: 10.1128/mcb.22.11.3864-3874.2002.
- Reimold AM, Etkin A, Clauss I, Perkins A, Friend DS, Zhang J, Horton HF, Scott A, Orkin SH, Byrne MC, et al. An essential role in liver development for transcription factor XBP-1. *Genes Dev*. 2000;14:152–157.
- Jin JK, Blackwood EA, Azizi K, Thuerlauf DJ, Fahem AG, Hofmann C, Kaufman RJ, Doroudgar S, Glembotski CC. ATF6 decreases myocardial ischemia/reperfusion damage and links ER stress and oxidative stress signaling pathways in the heart. *Circ Res*. 2017;120:862–875. DOI: 10.1161/CIRCRESAHA.116.310266.
- Yoshikawa A, Kamide T, Hashida K, Ta HM, Inahata Y, Takarada-Iemata M, Hattori T, Mori K, Takahashi R, Matsuyama T, et al. Deletion of Atf6alpha impairs astroglial activation and enhances neuronal death following brain ischemia in mice. *J Neurochem*. 2015;132:342–353. DOI: 10.1111/jnc.12981.
- Shen Y, Yan B, Zhao Q, Wang Z, Wu J, Ren J, Wang W, Yu S, Sheng H, Crowley SD, et al. Aging is associated with impaired activation of protein homeostasis-related pathways after cardiac arrest in mice. *J Am Heart Assoc*. 2018;7:e009634. DOI: 10.1161/JAHA.118.009634.
- Kumar R, Krause GS, Yoshida H, Mori K, DeGracia DJ. Dysfunction of the unfolded protein response during global brain ischemia and reperfusion. *J Cereb Blood Flow Metab*. 2003;23:462–471. DOI: 10.1097/01.WCB.0000056064.25434.CA.
- Yu Z, Sheng H, Liu S, Zhao S, Glembotski CC, Warner DS, Paschen W, Yang W. Activation of the ATF6 branch of the unfolded protein response in neurons improves stroke outcome. *J Cereb Blood Flow Metab*. 2017;37:1069–1079. DOI: 10.1177/0271678X16650218.
- Blackwood EA, Azizi K, Thuerlauf DJ, Paxman RJ, Plate L, Kelly JW, Wiseman RL, Glembotski CC. Pharmacologic atf6 activation confers global protection in widespread disease models by reprogramming cellular proteostasis. *Nat Commun*. 2019;10:187. DOI: 10.1038/s41467-018-08129-2.
- Blackwood EA, Hofmann C, Santo Domingo M, Bilal AS, Sarakki A, Stauffer W, Arrieta A, Thuerlauf DJ, Kolkhorst FW, Müller OJ, et al. ATF6 regulates cardiac hypertrophy by transcriptional induction of the mTORC1 activator, Rheb. *Circ Res*. 2019;124:79–93. DOI: 10.1161/CIRCRESAHA.118.313854.
- Glembotski CC. Roles for ATF6 and the sarco/endoplasmic reticulum protein quality control system in the heart. *J Mol Cell Cardiol*. 2014;71:11–15. DOI: 10.1016/j.jmcc.2013.09.018.
- Zhao Q, Shen Y, Li R, Wu J, Lyu J, Jiang M, Lu L, Zhu M, Wang W, Wang Z, et al. Cardiac arrest and resuscitation activates the hypothalamic-pituitary-adrenal axis and results in severe immunosuppression. *J Cereb Blood Flow Metab*. 2021;41:1091–1102. DOI: 10.1177/0271678X20948612.
- Liu H, Yu Z, Li Y, Xu B, Yan B, Paschen W, Warner DS, Yang W, Sheng H. Novel modification of potassium chloride induced cardiac arrest model for aged mice. *Aging Dis*. 2018;9:31–39. DOI: 10.14336/AD.2017.0221.
- Li R, Shen Y, Li X, Lu L, Wang Z, Sheng H, Hoffmann U, Yang W. Activation of the XBP1s/O-GlcNAcylation pathway improves functional

- outcome after cardiac arrest and resuscitation in young and aged mice. *Shock*. 2021. DOI: 10.1097/shk.0000000000001732.
22. Yu S, Galeffi F, Rodriguez RM, Wang Z, Shen Y, Lyu J, Li R, Bernstock JD, Johnson KR, Liu S, et al. Small ubiquitin-like modifier 2 (SUMO2) is critical for memory processes in mice. *FASEB J*. 2020;34:14750–14767. DOI: 10.1096/fj.20200850RR.
 23. Ruggiano A, Foresti O, Carvalho P. Quality control: ER-associated degradation: protein quality control and beyond. *J Cell Biol*. 2014;204:869–879. DOI: 10.1083/jcb.201312042.
 24. Belmont PJ, Chen WJ, San Pedro MN, Thuerauf DJ, Gellings Lowe N, Gude N, Hilton B, Wolkowicz R, Sussman MA, Glembotski CC. Roles for endoplasmic reticulum-associated degradation and the novel endoplasmic reticulum stress response gene Derlin-3 in the ischemic heart. *Circ Res*. 2010;106:307–316. DOI: 10.1161/CIRCRESAHA.109.203901.
 25. Eura Y, Miyata T, Kokame K. Derlin-3 is required for changes in ERAD complex formation under ER stress. *Int J Mol Sci*. 2020;21:6146. DOI: 10.3390/ijms21176146.
 26. Doroudgar S, Völkers M, Thuerauf DJ, Khan M, Mohsin S, Respress JL, Wang W, Gude N, Müller OJ, Wehrens XHT, et al. Hrd1 and ER-associated protein degradation, ERAD, are critical elements of the adaptive ER stress response in cardiac myocytes. *Circ Res*. 2015;117:536–546. DOI: 10.1161/CIRCRESAHA.115.306993.
 27. Liu S, Sheng H, Yu Z, Paschen W, Yang W. O-linked beta-N-acetylglucosamine modification of proteins is activated in post-ischemic brains of young but not aged mice: implications for impaired functional recovery from ischemic stress. *J Cereb Blood Flow Metab*. 2016;36:393–398. DOI: 10.1177/0271678X15608393.
 28. Iwabuchi M, Sheng H, Thompson JW, Wang L, Dubois LG, Gooden D, Moseley M, Paschen W, Yang W. Characterization of the ubiquitin-modified proteome regulated by transient forebrain ischemia. *J Cereb Blood Flow Metab*. 2014;34:425–432. DOI: 10.1038/jcbfm.2013.210.
 29. Akutsu M, Dikic I, Bremm A. Ubiquitin chain diversity at a glance. *J Cell Sci*. 2016;129:875–880. DOI: 10.1242/jcs.183954.
 30. Plate L, Cooley CB, Chen JJ, Paxman RJ, Gallagher CM, Madoux F, Genereux JC, Dobbs W, Garza D, Spicer TP, et al. Small molecule proteostasis regulators that reprogram the ER to reduce extracellular protein aggregation. *Elife*. 2016;5:e15550. DOI: 10.7554/eLife.15550.
 31. Thuerauf DJ, Morrison LE, Hoover H, Glembotski CC. Coordination of atf6-mediated transcription and ATF6 degradation by a domain that is shared with the viral transcription factor, VP16. *J Biol Chem*. 2002;277:20734–20739. DOI: 10.1074/jbc.M201749200.
 32. Yoshida H, Matsui T, Hosokawa N, Kaufman RJ, Nagata K, Mori K. A time-dependent phase shift in the mammalian unfolded protein response. *Dev Cell*. 2003;4:265–271. DOI: 10.1016/S1534-5807(03)00022-4.
 33. Eura Y, Yanamoto H, Arai Y, Okuda T, Miyata T, Kokame K. Derlin-1 deficiency is embryonic lethal, Derlin-3 deficiency appears normal, and Herp deficiency is intolerant to glucose load and ischemia in mice. *PLoS One*. 2012;7:e34298. DOI: 10.1371/journal.pone.0034298.
 34. Newton K, Matsumoto ML, Wertz IE, Kirkpatrick DS, Lill JR, Tan J, Dugger D, Gordon N, Sidhu SS, Fellouse FA, et al. Ubiquitin chain editing revealed by polyubiquitin linkage-specific antibodies. *Cell*. 2008;134:668–678. DOI: 10.1016/j.cell.2008.07.039.
 35. Lindholm P, Peranen J, Andressoo JO, Kalkkinen N, Kokaia Z, Lindvall O, Timmusk T, Saarna M. MANF is widely expressed in mammalian tissues and differently regulated after ischemic and epileptic insults in rodent brain. *Mol Cell Neurosci*. 2008;39:356–371. DOI: 10.1016/j.mcn.2008.07.016.
 36. Tadimalla A, Belmont PJ, Thuerauf DJ, Glassy MS, Martindale JJ, Gude N, Sussman MA, Glembotski CC. Mesencephalic astrocyte-derived neurotrophic factor is an ischemia-inducible secreted endoplasmic reticulum stress response protein in the heart. *Circ Res*. 2008;103:1249–1258. DOI: 10.1161/CIRCRESAHA.108.180679.
 37. Mätlik K, Anttila JE, Kuan-Yin T, Smolander O-P, Pakarinen E, Lehtonen L, Abo-Ramadan U, Lindholm P, Zheng C, Harvey B, et al. Poststroke delivery of MANF promotes functional recovery in rats. *Sci Adv*. 2018;4:eaap8957. DOI: 10.1126/sciadv.aap8957.
 38. Yan Y, Rato C, Rohland L, Preissler S, Ron D. MANF antagonizes nucleotide exchange by the endoplasmic reticulum chaperone BiP. *Nat Commun*. 2019;10:541. DOI: 10.1038/s41467-019-08450-4.
 39. Arrieta A, Blackwood EA, Stauffer WT, Santo Domingo M, Bilal AS, Thuerauf DJ, Pentoney AN, Aivati C, Sarakki AV, Doroudgar S, et al. Mesencephalic astrocyte-derived neurotrophic factor is an ER-resident chaperone that protects against reductive stress in the heart. *J Biol Chem*. 2020;295:7566–7583. DOI: 10.1074/jbc.RA120.013345.

Supplemental Material

Table S1. Animal summary of the CA outcome experiments.

Experiment	Groups	Total (n)	Exclusion criteria			Functional test (n)
			CPR	Death	Others	
Figure 1	Control vs KI	Control (n=12) KI (n=11)	1	Control (n=2) KI (n=1)	–	Control (n=9) KI (n=10)
Figure S1	Control vs KI	Control (n=9) KI (n=7)	–	Control (n=5) KI (n=1)	–	Control (n=4) KI (n=6)
Figure 6	Vehicle vs 147	Control (n=11) #147 (n=10)	–	Control (n=7) #147 (n=2)	–	Control (n=4) #147 (n=8)

KI: sATF6-KI mice.

Table S2. List of PCR primer sequences.

Purpose	Gene	Primer sequences (5'→3')
Genotyping	<i>Atf6</i>	Forward: CACTTGCTCTCCCAAAGTCG Reverse: GTTATGTAACGCGGAACTCC
	<i>Cre</i>	Forward: GGTGATGCAACGAGTGATGAGG Reverse: GCCAGATTACGTATATCCTGGCAG
qRT-PCR	<i>Hspa5 (GRP78)</i>	Forward: CGTATGTGGCCTTCACTCCT Reverse: TTTCTTCTGGGGCAAATGTC
	<i>P4hb (PDI)</i>	Forward: GAGGACAACGTCCTGGTGTT Reverse: GCCTTCTGCCTTCAGTTTTG
	<i>Pdia4 (ERp72)</i>	Forward: GTGGTCATCATTGGGCTCTT Reverse: CTTCTCAGGGTGTGTCAGCA
	<i>Derl3</i>	Forward: TCAACTTCTTCGGCTTACTCAAC Reverse: GGGAAGGGGCAGGTAATCG
	<i>Sdf2l1</i>	Forward: TGCACTCACACGACATCAAA Reverse: GACTGTCCACAGGTCCAGGT
	<i>Manf</i>	Forward: GCAAGAGGCAAAGAGAATCG Reverse: GTCCACTGTGCTCAGGTCAA
	<i>Dnajc3 (P58^{IPK})</i>	Forward: AAGCGGTGTTTTGCACACTA Reverse: TGCTCCTGAGCAGCTTCATA
	<i>Hyou1</i>	Forward: CCACATCAACTACGGTGACCT Reverse: CCAAACAGGCTGGATATGGT
	<i>Herpud1 (HERP)</i>	Forward: GCAGTTGGAGTGTGAGTCG Reverse: TCTGTGGATTTCAGCACCCCTTT
	<i>Pdia3</i>	Forward: TATGAAGCTGCAGCAACCAG Reverse: TGCTGGCTGCTTTTAGGAAT
	<i>Hrd1</i>	Forward: AACATCTCCTGGCTCTTCCA Reverse: GGCAAAGAGTGGGAATGTGT
	<i>Edem1</i>	Forward: GCATGTTTCGTCTTCGGCTAT Reverse: AGCTTCGAAGACCTGGACTG
	<i>β-actin</i>	Forward: TAGGCACCAGGGTGTGATG Reverse: GGGGTGTTGAAGGTCTCAA

Table S3. List of primary antibodies.

Antibody (Cat. #)	Species	Manufacturer
p-eIF2 α (9721)	Rabbit	Cell Signaling Technology
PERK (3192)	Rabbit	Cell Signaling Technology
eIF2 α (9722)	Rabbit	Cell Signaling Technology
GRP78 (610978)	Mouse	BD Biosciences
Ubiquitin (3936)	Mouse	Cell Signaling Technology
K48-Ubiquitin (8081)	Rabbit	Cell Signaling Technology
K63-Ubiquitin (5621)	Rabbit	Cell Signaling Technology
VCP (2648)	Rabbit	Cell Signaling Technology
Sel1l (sc-377350)	Mouse	Santa Cruz Biotechnology
HERP (sc-100721)	Mouse	Santa Cruz Biotechnology
OS9 (12497)	Rabbit	Cell Signaling Technology
Derl1 (NB100-448)	Rabbit	Novus Biologicals
MANF (AF3748)	Goat	Novus Biologicals
FLAG (F3165)	Mouse	Sigma
β -actin (A3854)	Mouse	Sigma

Table S4. Expression changes of major ERAD-related genes in sATF6-KI mouse brains revealed by our RNA-Seq analysis.

GeneID	Gene Name	Fold change	<i>padj</i>
ENSMUSG00000009092	Derl3	89.88	< 0.001
ENSMUSG00000026864	Hspa5 (GRP78)	5.41	< 0.001
ENSMUSG00000031770	Herpud1 (HERP)	4.02	< 0.001
ENSMUSG00000020964	Sel1l	2.70	< 0.001
ENSMUSG00000040462	Os9	1.94	< 0.001
ENSMUSG00000028452	Vcp	1.61	< 0.001
ENSMUSG00000024807	Syvn1 (Hrd1)	1.47	< 0.001
ENSMUSG00000018442	Derl2	1.47	< 0.001
ENSMUSG00000030104	Edem1	1.32	< 0.001
ENSMUSG00000022365	Derl1	1.16	0.110
ENSMUSG00000043019	Edem3	1.04	0.805
ENSMUSG00000025873	Faf2	1.03	0.871
ENSMUSG00000028277	Ube2j1	1.02	0.922
ENSMUSG00000020311	Erlec1	1.01	0.968
ENSMUSG00000023286	Ube2j2	-1.02	0.935
ENSMUSG00000038312	Edem2	-1.02	0.932
ENSMUSG00000039703	Nploc4	-1.04	0.805
ENSMUSG00000039100	March6	-1.04	0.730
ENSMUSG00000005262	Ufd1l	-1.06	0.645
ENSMUSG00000020794	Ube2g1	-1.06	0.649
ENSMUSG00000031751	Amfr	-1.09	0.363
ENSMUSG00000009293	Ube2g2	-1.14	0.230

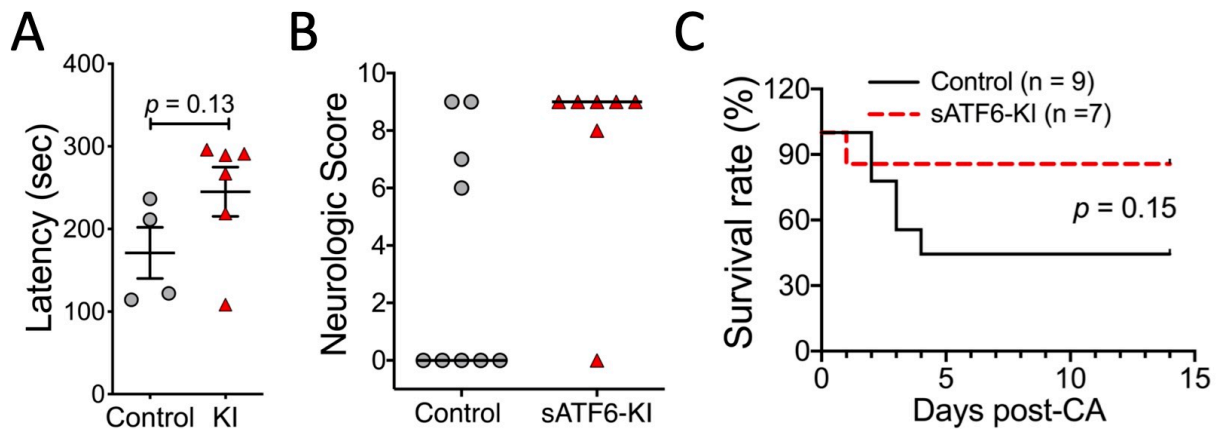


Figure S1. The effect of neuron-specific activation of the ATF6 UPR branch on long-term outcome after CA. Littermate control and sATF6-KI (KI) mice were treated with tamoxifen for 5 days. Three days later, the mice (n = 7-9/group) were subjected to 8.5 min CA. Rotarod (A) and neurologic score (B) was evaluated on day 7 after CA/CPR. For neurologic scores, dead mice (5 in vehicle group and 1 in sATF6-KI group) were also shown in the figure (score = 0), and were excluded for statistical analysis. (C) Survival rates during the 14-day observation after CA/CPR (log-rank test). Data are presented as mean \pm SEM, median, or percentage.

Figure S2. Gene ontology (GO) and IPA analyses of differentially expressed genes (DEGs) between control and sATF6-KI mice. (A) Top over-represented GO terms (p threshold < 0.01) (B) Top 10 enriched canonical pathways revealed by IPA analysis. The bar charts represent the $-\log_{10}$ (p -value) calculated based on Fisher's exact test. BP: biological process; CC: cellular component; MF: molecular function.